Cross Sections of Nuclei for High-Energy Pions*

J. W. CRONIN, R. COOL, AND A. ABASHIAN†
Brookhaven National Laboratory, Upton, New York
(Received May 14, 1957)

Measurements of the diffraction and absorption cross sections of nuclei for negative pions at kinetic energies between 0.6 and 1.4 Bev are described. They include the absorption cross section (1) in selected nuclei from Be to Pb at 0.97 Bev, (2) in C between 0.6 and 1.2 Bev, and (3) in Al, Ca, and Pb for 1.5-Bev/c momentum π^- and protons. Diffraction cross sections were obtained for (1) Be, C, Al, and Ca at 0.97 Bev and (2) C at 0.6, 0.8, and 1.2 Bev.

The data are compared to the optical model of the nucleus. Detailed computations are described both for a tapered Fermi-type distribution of nucleons which fits the high-energy electron scattering data and for a uniform square-well nucleon distribution of the form $R=r_0A^{\frac{1}{3}}$. All of the absorption cross sections are shown to be in excellent agreement for a Fermi distribution with a single radial parameter $c=(1.14\pm0.04)A^{\frac{1}{3}}\times10^{-13}$ cm, which is 6% larger than that required by electromagnetic measurements. The data are also consistent with the same value of the radial parameter as that which fits the electron-scattering data if the range of the pion-nucleon force is taken to be $\approx1.0\times10^{-13}$ cm. This range is equal to the range required by pion-nucleon scattering data. A uniform distribution $R=r_0A^{\frac{1}{3}}$ is not consistent with the data.

The diffraction cross sections appear to be 20–30% higher than those predicted by the optical model and the dispersion relations. The implications of this discrepancy are discussed.

I. INTRODUCTION

THE absorption and diffraction cross sections of selected nuclei have been measured by using negative pions at kinetic energies between 0.6 and 1.4 Bev. These cross sections yield information concerning the size, shape, and strength of the pion-nucleus potential. Some data are already available in the Bev range for neutrons and protons.[1]

The usual interpretation of nuclear cross sections at high energies has been made in terms of the optical model originally proposed by Fernbach, Serber, and Taylor.[2] This model has been extended and generalized by many other authors.[3] As is well known, the model assumes that the detailed structure of the nucleus can be described approximately by an average potential. The real and imaginary parts of this potential then give the diffraction cross section σ_d and the absorption cross section σ_a.

On the basis of general quantum-mechanical principles,[4] the strength of the potential is related to the real and imaginary forward scattering amplitudes of the elementary pion-nucleon interaction. For pions, the real and imaginary forward scattering amplitudes are known as a function of energy.[5] The imaginary part is given by $\mathrm{Im}f(0)=\sigma/4\pi\lambda$, where σ is the pion-nucleon total cross section. The real part has been obtained by the application of the dispersion relations.[6] Thus, to the extent that the potential description is valid, both the absorption and diffraction cross sections can be computed and they depend only upon the shape and radius of the potential.[7]

The measurement of the elastic scattering of high-energy electrons by Hofstadter and co-workers[8] has given very accurate values for the radius and shape of the nuclear charge distribution. For medium and heavy nuclei, they find that the charge density distribution can be represented by a Fermi-type distribution

$$\rho_{\mathrm{em}}(r)=\rho_0/\{\exp[(r-c)/z]+1\}, \qquad (1)$$

where $c=1.08A^{\frac{1}{3}}\times10^{-13}$ cm, $z=0.53\times10^{-13}$ cm, and ρ_0 is the charge density at $r=0$. In the approximation that the proton is a point charge, $\rho_{\mathrm{em}}(r)$ is also the spatial distribution of the protons $\rho(r)$.

A difference in the radii of neutron and proton distributions should be revealed by a comparison of the π^+ and π^- absorption cross sections at suitable energies.[9] Results of such an experiment have already been published.[10] They show that the difference is less than 3% in radius for Pb. Therefore we shall assume in the following that the radial distributions of the protons and neutrons are identical, which is sufficiently accurate for our purpose.

The optical-model nuclear potential can then be

* Work performed under the auspices of the U. S. Atomic Energy Commission.

† In partial fulfillment of the requirements for the degree of Doctor of Philosophy at The Johns Hopkins University.

[1] Chen, Leavitt, and Shapiro, Phys. Rev. **99**, 857 (1955); Coor, Hill, Hornyak, Smith, and Snow, Phys. Rev. **98**, 1369 (1955); Booth, Ledley, Walker, and White, Proc. Phys. Soc. (London) **A 70**, 209 (1957).

[2] Fernbach, Serber and Taylor, Phys. Rev. **75**, 1352 (1949), henceforth referred to as FST.

[3] K. M. Watson, Phys. Rev. **89**, 575 (1953); N. C. Francis and K. M. Watson, Phys. Rev. **92**, 291 (1953); G. Takeda and K. M. Watson, Phys. Rev. **97**, 1336 (1955); K. M. Watson, Phys. Rev. **105**, 1388 (1957); Frank, Gammel, and Watson, Phys. Rev. **101**, 891 (1956); L. S. Kisslinger, Phys. Rev. **98**, 768 (1955); W. W. Wada, Phys. Rev. **92**, 152 (1953).

[4] H. A. Bethe and R. R. Wilson, Phys. Rev. **83**, 690 (1951).

[5] Cool, Piccioni, and Clark, Phys. Rev. **103**, 1082 (1956).

[6] R. Karplus and M. A. Ruderman, Phys. Rev. **98**, 771 (1955); M. L. Goldberger, Phys. Rev. **99**, 979 (1955); Goldberger, Miyazawa, and Oehme, Phys. Rev. **99**, 986 (1955); Anderson, Davidon, and Kruse, Phys. Rev. **100**, 339 (1955); R. M. Sternheimer, Phys. Rev. **101**, 384 (1956).

[7] R. M. Sternheimer, Phys. Rev. **101**, 384 (1956); Frank, Gammel, and Watson, Phys. Rev. **101**, 891 (1956).

[8] R. Hofstadter, Revs. Modern Phys. **28**, 214 (1956). References to other data on electromagnetic interaction radii are contained therein.

[9] E. D. Courant, Phys. Rev. **94**, 1081 (1954).

[10] Abashian, Cool, and Cronin, Phys. Rev. **104**, 855 (1956); see also W. N. Hess and B. J. Moyer, Phys. Rev. **101**, 337 (1956); R. W. Williams, Phys. Rev. **98**, 1387 (1955).

written in the form

$$V_N(r) = V_0\rho(r). \quad (2)$$

From the pion scattering and absorption cross section one can, in principle, determine $V_N(r)$. In practice, however, our measurements are not sufficiently accurate to obtain both the radius and the shape of the potential. Therefore, we shall assume that $\rho(r)$ has the functional form of Eq. (1) and has the same value of the fall-off parameter z as that obtained from the electron-scattering data. In effect, we assume that the finite range of the nuclear force does not appreciably alter the fall-off distance of the potential. Our measurements thus lead to values of the parameter c for the nuclear potential. We also compare our results to those expected on the basis of a uniform distribution (square-well potential).

II. EXPERIMENTAL PROCEDURE

To compare the measured cross sections with the predictions of the optical model, it would be most convenient to obtain the diffraction and absorption cross sections separately. A measurement at each angle of the momentum distribution of the scattered particles, made with sufficient resolution, will in principle completely separate the processes. The limited intensity of high-energy pion beams, as well as the difficulty in obtaining sufficient resolution at this energy, makes this method impractical. However, at these high energies, the diffraction scattering is confined to a relatively small solid angle near the forward direction, while the secondaries of inelastic interactions are more uniformly spread. Moreover, the angular distribution of the diffraction scattering is calculable from the theory of the optical model. It is thus possible, as the results will show, to make a separation by a measurement of the angular distribution alone. For practical reasons, we have chosen to measure the integral angular distribution; that is, we have determined the attenuation of a well-defined beam in an absorber as a function of the half-angle θ subtended by a large counter connected in anticoincidence with a beam-defining telescope.[11] The data which we obtain are thus the fraction of the incident beam that scatters or interacts in an absorber for which no charged secondary particle falls within a cone of semiaperture θ. For each absorber and beam condition chosen, we vary the angle θ over a suitable range, as will be discussed in Sec. IID.

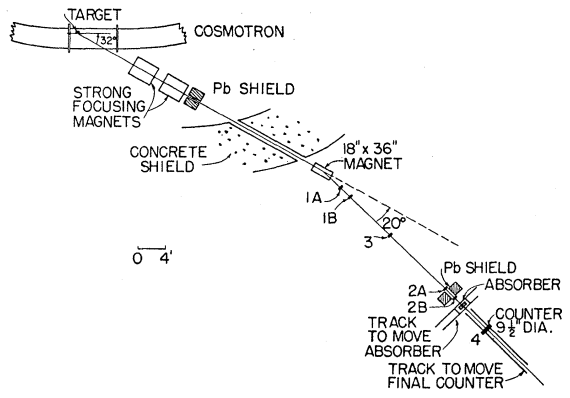

FIG. 1. Schematic arrangement of the apparatus.

A. Beams

The pion beams were produced by 3-Bev protons striking a beryllium target in a field-free section of the Cosmotron. The experimental arrangement is shown in Fig. 1. A beam of secondary particles was selected at an angle of 32° to the incident proton direction. The beam was focused by a 12-in. diameter strong-focusing magnetic lens and was momentum-analyzed by magnetic deflection through an angle of 20°. It was defined by a telescope consisting of five scintillation counters. Counters $1A$, $1B$, and 3 (see Fig. 1) were $3\frac{1}{2}$-in. diameter plastic scintillators; counter $2A$ was 3 in. in diameter; counter $2B$ was either 3 in., 2 in., or 1 in. in diameter, depending on the beam size desired. The momentum resolution for the arrangement shown with a 3-in. counter at $2B$ was calculated to be $\pm 2\%$. When the magnets were adjusted to select negative particles, the beam consisted mainly of negative pions with a small muon contamination (see Sec. IIE). When positive particles were selected, the beam contained both protons and positive pions. To obtain a pure proton beam at 1.5-Bev/c momentum, the proton energy incident on the target was reduced to 1.25-Bev kinetic energy, which is below the threshold for producing pions of 1.5 Bev/c. The mean value of the momentum selected by the apparatus was calibrated by a current carrying wire to an estimated accuracy of $\pm 1.5\%$. The intensity of the circulating beam of the Cosmotron was adjusted to give ≈ 400 counts per pulse of 10 milliseconds duration.

B. Anticoincidence Counter

The center of each absorber was placed 12 in. behind counter $2B$ on a cart which could be readily moved in or out of the beam. The attenuation was measured by a $9\frac{1}{2}$-in. diameter counter (shown as number 4 in Fig. 1) connected in anticoincidence with the beam telescope. This counter was a $2\frac{1}{2}$-in. thick cylindrical container filled with a toluene-terphenyl mixture and was viewed by four RCA 6342 photomultiplier tubes. The half-angle θ subtended by counter 4 at the absorber could be varied from 2.5° to 20° by moving it along a track in line with the beam. The spatial distribution of the beam was measured at the smallest and largest angle positions by means of a small probe counter. Thus, counter 4 was

[11] A similar technique has been used by Chen, Leavitt, and Shapiro, Phys. Rev. 99, 857 (1955).

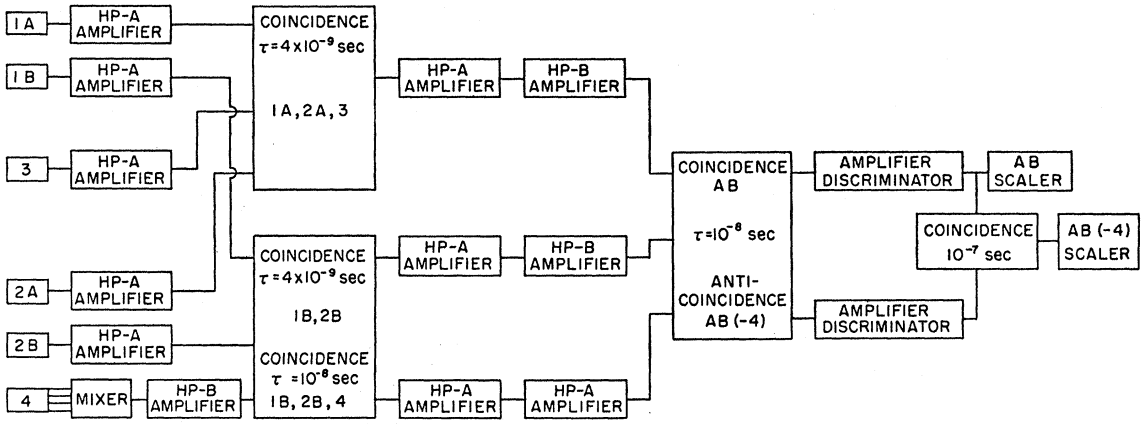

FIG. 2. Block diagram of the electronic circuits.

accurately centered on the beam over its entire range of motion.

Tests were performed to determine whether counter 4 was uniformly efficient over its entire geometrical area. The beam defined by the telescope was spread over the surface of the counter by the multiple Coulomb scattering in 1.5 in. Pb. A small 1-in. square probe counter, located behind counter 4, was operated in coincidence with the beam-defining telescope. The anticoincidence rate of counter 4 then measured its inefficiency at the location of the probe counter. The efficienty of the counter was mapped and found uniform over its entire surface. The efficienty was greater than 98%.

C. Electronics

The electronic circuits are similar to those previously described.[5] Figure 2 shows a block diagram of the arrangement. Since the singles counting rate of counter 4 was high ($\approx 2\times 10^6$ sec^{-1}), special precautions were taken to minimize dead-time losses in this channel. A test of its efficiency as a function of counting rate was made. The efficiency was found to be constant over the range of counting rates used.

Accidental coincidence rates were measured by inserting artificial delays in various branches of the electronic circuits. Only those resulting from the high singles rate in counter 4 were appreciable. By shielding it with a collimator (shown in Fig. 1 near counters $2A$ and $2B$) from most of the particles which do not pass through the telescope, the singles rate was reduced. The chance coincidence rate was then less than 2%.

D. Measurements

The elements used were approximately uniformly spaced in $A^{\frac{1}{3}}$. The chemical purity of all samples was greater than 99%. The thickness in g cm^{-2} was measured to an accuracy of $\pm 0.5\%$. The thickness of the absorber selected in the case of heavier elements was limited by the requirement that loss of beam due to multiple Coulomb scattering be negligible. For the light elements, the thickness was chosen to absorb about 20% of the beam. For a given absorber thickness and sufficiently small angle θ, the anticoincidence rate due to multiple Coulomb scattering becomes a large fraction of the apparent absorption. In principle, a correction for this effect could be calculated from the thickness of the absorber and the beam distribution.[12] However, the calculation of this correction is very sensitive to the exact beam distribution. It was impractical to measure the distribution to the required accuracy because the apparent absorption due to Coulomb scattering very rapidly becomes large compared to the nuclear cross section as the angle is decreased. On the other hand, the angle θ at which multiple Coulomb scattering losses become important can be readily determined experimentally for an absorber of given thickness in radiation lengths. We have made absorption measurements with Pb of 0.5 and 2.0 radiation lengths as a function of θ for both 2-in. and 3-in. counters at position $2B$. Figure 3 shows a typical result. The angle at which this curve begins to rise rapidly is considerably greater than that expected for nuclear diffraction scattering and the rise is therefore clearly to be identified with Coulomb scattering. From this curve one thus establishes, for

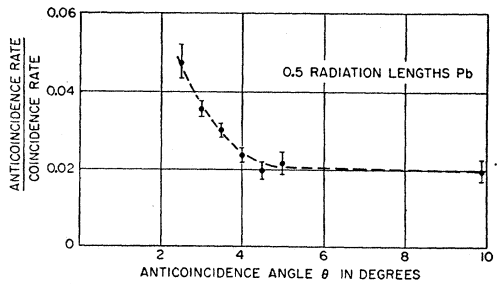

FIG. 3. Loss of beam at small angles from multiple Coulomb scattering for a Pb absorber of 0.5 radiation length. The flat portion of the curve at angles greater than ~4° is due to nuclear absorption.

[12] R. M. Sternheimer, Rev. Sci. Instr. 25, 1070 (1954).

example, that the loss at 4° is 0.5% of the beam for 0.5 radiation length of absorber. In our measurements, the angles were always chosen such that the multiple Coulomb scattering loss was less than 0.5% of the beam. This choice prevented the measurement of the diffraction cross section for elements heavier than Ca. Interference effects between Coulomb and diffraction scattering will be discussed in Sec. IV.

Measurements of the attenuation as a function of θ were made for each element from the minimum angle defined by Coulomb scattering loss to a maximum angle of 15°–20°. At each angle, a measurement consisted of several short runs of target in and target out to avoid errors due to possible slow drifts in the electronic apparatus. Subsequent statistical analysis of the data did not, in fact, reveal any significant effect of this kind.

Measurements on Be, C, Al, Ca, Cu, Sn, and Pb were made for 970-Mev negative pions. Carbon was also measured at negative pion energies of 600, 800, and 1200 Mev. Measurements on Pb, Ca, and Al were made for both negative pions and protons of 1500-Mev/c momentum in identical geometry.

TABLE I. The measured attenuation cross sections of negative pions as a function of the anticoincidence angle.

Kinetic energy Bev (lab)	Element	Absorber thickness (g cm^{-2})	Anti-coincidence angle θ (degrees)	Diameter of counter $2B$ (inches)	Measured cross section (mb)	Statistical probable error (mb)
0.97	Be	18.75	2.89	3.0	260	3.0
0.97	Be	18.75	4.15	3.0	238	2.7
0.97	Be	18.75	6.48	3.0	231	2.6
0.97	Be	18.75	10.10	3.0	186	2.4
0.97	Be	18.75	14.30	3.0	165	2.1
0.97	Be	18.75	18.15	3.0	150	2.0
0.97	C	16.88	2.64	3.0	334	5.3
0.97	C	16.88	3.95	3.0	300	5.0
0.97	C	16.88	5.92	3.0	275	3.8
0.97	C	16.88	9.72	3.0	239	3.9
0.97	C	16.88	12.95	3.0	212	3.1
0.97	C	16.88	16.50	3.0	190	3.8
0.97	Al	10.30	4.00	2.0	559	8.3
0.97	Al	10.30	5.25	2.0	509	7.4
0.97	Al	10.52	7.17	3.0	444	15
0.97	Al	10.30	9.10	2.0	438	7.0
0.97	Al	10.52	9.38	3.0	418	13
0.97	Al	10.30	13.50	2.0	379	7.4
0.97	Al	10.30	17.60	2.0	343	7.4
0.97	Ca	5.11	3.71	3.0	798	31
0.97	Ca	7.44	4.00	1.0	778	23
0.97	Ca	5.11	6.33	3.0	586	27
0.97	Ca	7.44	8.10	1.0	612	22
0.97	Ca	5.11	8.78	3.0	626	25
0.97	Ca	5.11	10.90	3.0	599	25
0.97	Ca	7.44	15.60	1.0	492	21
0.97	Cu	22.01	7.00	2.0	854	9.6
0.97	Cu	11.36	7.56	3.0	789	20
0.97	Cu	11.36	9.39	3.0	780	18
0.97	Cu	22.01	10.30	2.0	775	8.6
0.97	Cu	22.01	13.70	2.0	718	9.1
0.97	Sn	18.30	6.95	3.0	1240	23
0.97	Sn	18.30	7.00	2.0	1309	22
0.97	Sn	18.30	8.00	3.0	1220	62
0.97	Sn	18.30	10.00	3.0	1174	22
0.97	Sn	18.30	10.30	2.0	1176	19
0.97	Sn	18.30	13.70	2.0	1113	19
0.97	Pb	14.18	7.00	2.0	1930	34
0.97	Pb	10.72	8.00	3.0	1758	67
0.97	Pb	14.18	10.30	2.0	1760	58
0.97	Pb	14.18	13.70	2.0	1654	34
0.60	C	16.88	6.16	3.0	257	3.0
0.60	C	16.88	14.00	3.0	199	3.3
0.60	C	16.88	24.30	3.0	173	2.8
0.80	C	16.88	4.84	3.0	299	5.1
0.80	C	16.88	11.20	3.0	231	3.8
0.80	C	16.88	18.75	3.0	196	3.1
1.20	C	16.88	3.13	3.0	315	6.0
1.20	C	16.88	8.00	3.0	239	4.7
1.20	C	16.88	13.35	3.0	203	3.5

E. Muon Contamination

Measurements with pions require a correction for the muon contamination in the beam. This correction was deduced by methods for which a detailed discussion has been given previously.[5] A range curve for the 970-Mev pion beam gave an upper limit of 0.031 for the fraction of muons originating from decays before the analyzing magnet and a lower limit of zero. The fraction of muons originating after the magnetic deflection was found to be 0.080 by an approximate calculation and by comparison with more precise UNIVAC computations described earlier.[5] Upon combining the two results, the muon contamination was taken to be 0.09±0.03. Previous experience has shown that the contamination varies little over the pion momenta used in this experiment. Hence, the same correction was applied at each momentum. Electron contaminations have been shown to be less than 1%.[5]

Table I and Table II list the results for the measured total cross sections. In Sec. IV the measured values will be separated into absorption and diffraction cross sections. The errors quoted are statistical standard deviations only and do not include the 3% uncertainty due to muon contamination.

III. CALCULATION OF CROSS SECTIONS FROM THE OPTICAL MODEL

In general, a free pion of wave number k_0 will have a wave number $k=k_0+k_1(\mathbf{r})+\frac{1}{2}iK(\mathbf{r})$ in a nuclear medium. For negative pions in a nucleus characterized by Z and A, the optical model predicts for $k_0\cong k$ that[2,3]

$$k_1(\mathbf{r})=[2\pi\rho(\mathbf{r})/k_0]\{[Z\alpha_r^-(0)+(A-Z)\alpha_r^+(0)]/A\}, \quad (3)$$

$$\tfrac{1}{2}K(\mathbf{r})=[2\pi\rho(\mathbf{r})/k_0]\{[Z\alpha_i^-(0)+(A-Z)\alpha_i^+(0)]/A\}, \quad (4)$$

TABLE II. The attenuation cross sections of negative pions and protons at momentum 1500 Mev/c.

Element	Absorber thickness (g cm^{-2})	Anti-coincidence angle θ (degrees)	Measured cross section for protons (mb)	Measured cross section for π^- (mb)
Al	31.12	9.2	416± 3.2	421±14
Al	31.12	17.6	317± 2.9	319±11
Ca	17.34	7.0	600± 7.0	607±22
Ca	17.34	10.3		524±28
Ca	17.34	13.7	490± 7.0	486±18
Pb	14.18	6.0	1870±36.0	1908±72
Pb	14.18	11.8	1651±32.0	1695±64

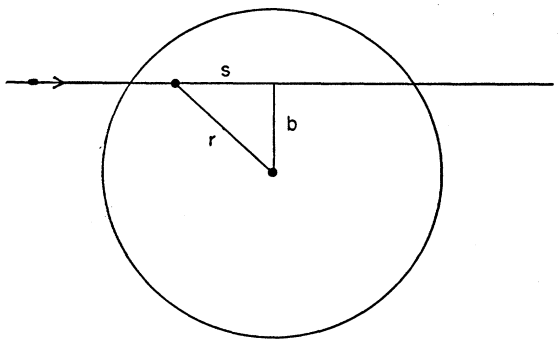

FIG. 4. The trajectory S of a particle passing through the nucleus in terms of r and b.

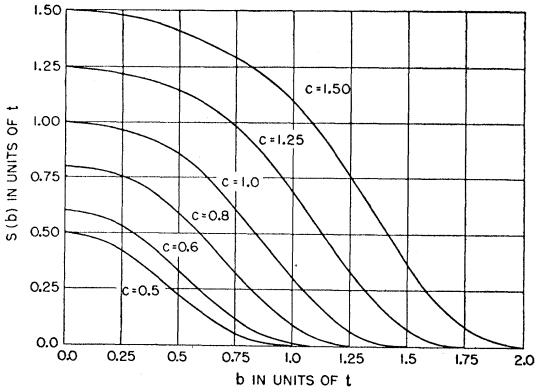

FIG. 5. The effective path length $S(b)$ as a function of b for the Fermi distribution. The curves are plotted for various values of the parameter c in Eq. (6). Units are in terms of the length t.

where $\rho(\mathbf{r})$ is the density of nucleons, $\alpha(0)$ is a pion-nucleon forward scattering amplitude, subscripts r and i indicate real and imaginary part, and superscripts $+$ and $-$ indicate π^+-p and π^--p amplitudes, respectively. Charge symmetry has been used to equate the π^--n amplitude to the π^+-p amplitude. Since $\alpha(0)=k_0\sigma_t/4\pi$, where σ_t is the pion-nucleon total cross section, substituting in Eq. (4) we have $K(\mathbf{r})=\rho(\mathbf{r})\bar{\sigma}$, where $\bar{\sigma}\equiv[Z\sigma_t^-+(A-Z)\sigma_t^+]/A$. For relativistic pions, the equivalent complex potential[13] is given by

$$V(\mathbf{r})=\hbar c\beta[k_1(\mathbf{r})+\tfrac{1}{2}iK(\mathbf{r})]. \tag{5}$$

The dispersion relations[6] give values for the real part of the forward scattering amplitude. They yield a value of k_1/K less than 0.1 for kinetic energies between 600 and 1500 Mev. The value of σ_d calculated for $k_1/K=0.1$ differs from that calculated for $k_1=0$ by less than 3%; hence to simplify the calculations they have been carried out for $k_1=0$.

For a square-well nucleon distribution, the cross sections can be calculated from formulas given by FST[2] in terms of $\bar{\sigma}$ and R, the radius of the nucleus. For the Fermi distribution, this computation can be carried out as follows: Eq. (1) is well approximated by $\rho(r)=\rho_0 u(r)$, where

$$\begin{aligned} &u(r)=1, \quad 0\leq r\leq c-\tfrac{1}{2}t \\ &u(r)=\tfrac{1}{2}-\tfrac{3}{2}\left(\frac{r-c}{t}\right)+2\left(\frac{r-c}{t}\right)^3, \quad c-\tfrac{1}{2}t\leq r\leq c+\tfrac{1}{2}t \\ &u(r)=0, \quad r\geq c+\tfrac{1}{2}t \end{aligned} \tag{6}$$

and ρ_0 is the density of nucleons at $r=0$. To fit the Hofstadter fall-off parameter $z=0.53\times10^{-13}$ cm, we must choose $t=4.23\times10^{-13}$ cm. This gives a 90% to 10% surface thickness of 2.5×10^{-13} cm. We shall define units of length in terms of t. The parameter c has the same meaning in Eqs. (1) and (6) and is the half-density radius. For example, to fit the Hofstadter parameter $c=1.07A^{\frac{1}{3}}\times10^{-13}$ cm, we have, in our units, $c=0.253A^{\frac{1}{3}}$. The distribution of Eq. (6) for Pb is identical to that used by Williams,[14] but differs for the lighter elements. The central density ρ_0 for the Fermi distribution is given by demanding that $\int\rho(r)4\pi r^2dr=A$, which leads to the result

$$\rho_0=A\left[4\pi\left(\frac{c^3}{3}+\frac{c}{20}\right)\right]^{-1} \tag{7}$$

in units of t.

The expressions for all cross sections contain the integral

$$\int_0^\infty Kds=\rho_0\bar{\sigma}\int_0^\infty u((s^2+b^2)^{\frac{1}{2}})ds, \tag{8}$$

where b is the impact parameter and s is the distance along the path defined by b (see Fig. 4). The integral on the right side of Eq. (8) is a function of b only, which we call $S(b)$, the effective path length in the nucleus. For the Fermi distribution, we have calculated $S(b)$ for values of c ranging from 0.5 to 1.5 which describe nuclei from Be to Pb. Figure 5 gives curves of $S(b)$ for different values of the parameter c.

The cross sections are then given by

$$\begin{aligned} \sigma_a&=2\pi\int_0^\infty\{1-\exp[-2\bar{\sigma}\rho_0S(b)]\}bdb, \\ \sigma_d&=2\pi\int_0^\infty\{1-\exp[-\bar{\sigma}\rho_0S(b)]\}^2bdb, \\ [d\sigma(\theta)/d\Omega]_d&=\left|k_0\int_0^\infty\{1-\exp[-\bar{\sigma}\rho_0S(b)]\}\right. \\ &\qquad\left.\times J_0(k_0b\sin\theta)bdb\right|^2. \end{aligned} \tag{9}$$

[13] Equation (5) is the correct form if the potential is expressed as the fourth component of a four-vector in a Klein-Gordon equation, and it is small compared to the total energy.

[14] R. W. Williams, Phys. Rev. **98**, 1387 (1955).

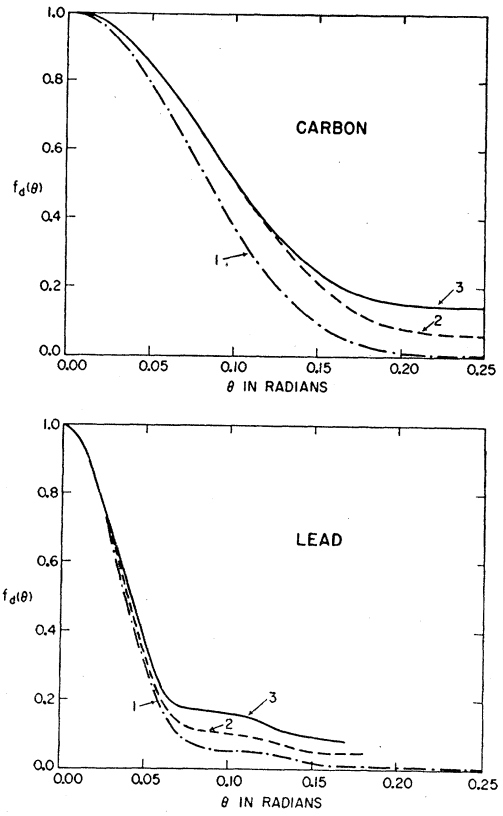

FIG. 6. The integral angular distribution $f_d(\theta)$, which is defined in Eq. (10), as a function of θ. The curves are plotted for C and Pb in the case of infinitely good angular resolution. Curves 1 are for a Fermi distribution with $c=1.13A^{\frac{1}{3}}\times10^{-13}$ cm and curves 2 for a uniform distribution with $r=1.3A^{\frac{1}{3}}\times10^{-13}$ cm and $\bar{\sigma}=32$ mb; curves 3 are for a uniform distribution with $r=1.3A^{\frac{1}{3}}\times10^{-13}$ cm when one assumes a completely opaque nucleus.

These cross sections have been evaluated by numerical integration. Figure 6 shows integrated curves of $[d\sigma(\theta)/d\Omega]_d$ for a typical set of parameters both for the Fermi and uniform distributions. The essential difference is that the Fermi distribution gives less large-angle diffraction scattering.

To deduce the diffraction cross sections from the data, it is necessary to compute the fraction of the scattering which fails to strike counter 4 when set at a given angle θ. The required integral, which takes into account the finite angular resolution, is

$$f_d(\theta)=2\pi\sigma_d^{-1}\int_0^\pi [d\sigma(\theta')/d\Omega]_d R(\theta-\theta')\sin\theta' d\theta'. \quad (10)$$

$R(\theta-\theta')$, which expresses the angular resolution, rises from zero at $\theta'=(\theta-\Delta\theta)$ to unity at $\theta'=(\theta+\Delta\theta)$ and remains unity thereafter. The form of the function R is obtained from the measured beam distribution. The value of $\Delta\theta/\theta$ was approximately 0.3.

TABLE III. The absorption and diffraction cross sections for 970-Mev negative pions. η is defined in Eq. (11′), Sec. IV.

Element	Absorption cross section σ_a in mb[a]	Diffraction cross section σ_d in mb	σ_d/σ_a	η barns sterad^{-1}
Be	197± 9	76±15	0.38±0.08	0.16±0.02
C	252± 13	78±21	0.31±0.08	0.24±0.03
Al	442± 20	217±41	0.49±0.09	0.35±0.05
Ca	618± 27	290±60	0.47±0.10	0.54±0.05
Cu	806± 35			0.64±0.11
Sn	1199± 52			0.69±0.19
Pb	1690±100			0.48±0.48

[a] A small electrostatic correction has been applied as explained in Sec. VA.

IV. ABSORPTION AND DIFFRACTION CROSS SECTIONS

To carry out the separation of $\sigma_m(\theta)$ into σ_a and σ_d in a systematic manner, we represent the measured cross section $\sigma_m(\theta)$ as

$$\sigma_m(\theta)=\sigma_a-\int_0^\theta [d\sigma(\theta)/d\Omega]_a d\Omega+f_d(\theta)\sigma_d, \quad (11)$$

where $[d\sigma(\theta)/d\Omega]_a$ is the angular distribution of the detectable charged secondaries resulting from absorptive collisions.

We shall assume that the angular distribution $f_d(\theta)$ is correctly given by the optical model. The form of $f_d(\theta)$ depends, of course, on the radius and form of the assumed potential as indicated in Sec. III. Thus, after assuming a trial radius and form of the potential, the resulting σ_a and σ_d must be compared to the predicted cross sections for the same potential. The consistency of σ_a and σ_d deduced in this way with the computed values then allows us to deduce the best radius and form of the potential.

Although the measurements at large angles indicate that $[d\sigma(\theta)/d\Omega]_a$ does not vary rapidly over this range of angles, we have no *a priori* knowledge of the form of this function from nuclear theory. For the purpose of extrapolating σ_a to zero angle, we shall assume that $[d\sigma(\theta)/d\Omega]_a$ is constant over the range of angles measured here. Fortunately one can easily show that for our purpose this approximation is very good if the true distribution does not vary too rapidly with decreasing angle. If the true distribution can be approximated in the form

$$[d\sigma(\theta)/d\Omega]_a=\textstyle\sum_n |a_n|\cos^n\theta, \quad (12)$$

then the error introduced in extrapolating to $\theta=0°$ from points at $\theta=7.5°$ and 15° is less than 2% for $n\leq12$. The rise in σ_m itself between 7.5° and 15° is considerably less rapid than $\cos^{12}\theta$ so the assumption seems well justified. There is some additional evidence, though indirect, from the high-energy secondaries generated by neutrons of ≈1.4 Bev.[1] Extrapolating this observed distribution to zero on the basis of our assumption would lead to an error of 1%.

In accord with the foregoing discussion, we have made a least-squares fit to our data of the form

$$\sigma_m(\theta)=f_d(\theta)\sigma_d+\sigma_a-2\pi\eta(1-\cos\theta), \quad (11')$$

TABLE IV. The absorption and diffraction cross sections for carbon as a function of energy. The computed values are for a Fermi distribution with $c=1.13A^{\frac{1}{3}}\times10^{-13}$ cm; the values of $\bar{\sigma}$ and k_1/K are given in the last columns.

Kinetic energy Mev (lab)	Measured absorption cross section σ_a in mb	Measured diffraction cross section σ_d in mb	Measured σ_d/σ_a	η barns sterad^{-1}	Computed absorption cross section σ_a in mb	Computed diffraction cross section σ_d in mb	$\bar{\sigma}$ mb	k_1/K
600	216±10	70±16	0.32±0.07	0.09±0.01	216	45	26	0.072
800	238±12	99±19	0.42±0.08	0.12±0.02	240	60	33	0.036
970	252±13	78±21	0.31±0.08	0.24±0.03	244	61	34	0.050
1200	246±14	105±22	0.43±0.09	0.26±0.05	236	59	32	0.076

in which the values of σ_d, σ_a, and η are then determined from the data. The results are given for the negative-pion data in Tables III and IV.

In elements heavier than Ca, the multiple Coulomb scattering effects discussed in Sec. IID, prevent us from obtaining a value for σ_d. For these elements, we must make some assumption about the value of σ_d in order to evaluate its contribution at large angles. For pions, as previously discussed, both the real and imaginary forward scattering amplitudes are known and σ_d can be calculated from the optical model. Moreover, at least for the light elements, our results for σ_d will be a check of the validity of this computation. It is easy to see that σ_a is not sensitive to the value of σ_d. For Pb, which is the worst case, σ_d contributes less than 3% at large angles while σ_d/σ_a is expected to be about 0.8; thus a 40% error in the value of σ_d would introduce an error of only 1% in the value of σ_a deduced.

In writing Eqs. (11) and (11′), we have neglected contributions from multiple and single Coulomb scattering for the reasons given in Sec. IID. This conclusion was based on measurements made in Pb at angles such that the coherent diffraction scattering amplitude $\alpha_n(\theta)$ was negligible. However, in the light elements where we wish to measure σ_d, the value of $\alpha_n(\theta)$ is not negligible. Thus, interference with the Coulomb amplitude may contribute to the measured cross section. It is possible to calculate approximately the contribution of such interference terms.[15] The result is that the contribution could be neglected except at the smallest angle measured for Ca. Therefore this angle was omitted in the analysis of the data.

V. RESULTS

A. Absorption Cross Sections for 970-Mev π^- Mesons

Table III gives the values deduced for σ_a at 970 Mev for the selected elements. The values of $\eta=[d\sigma(\theta)/d\Omega]_a$ for the charged secondaries of inelastic collisions are noted in the last column.

The function $f_d(\theta)$ in Eq. (11′), which was used to obtain the values of σ_a in the table, was that which applies for the Fermi distribution with $c=1.13A^{\frac{1}{3}}\times10^{-13}$ cm, $\bar{\sigma}=32$ mb, and $t=4.23\times10^{-13}$ cm. However, the values of σ_a are not sensitive to the model used in obtaining $f_d(\theta)$, since σ_a is principally determined at angles for which $f_d(\theta)$ is always small. For example, σ_a would be smaller by only 3% for a uniform distribution as can be seen directly from Fig. 6.

The error given for σ_a is an estimate of the systematic uncertainty compounded with the statistical errors from the least-squares analysis. The systematic error is an estimate of the uncertainty in extrapolation to zero angle as discussed in Sec. IV. The extrapolated correction to obtain $\sigma_a(0°)$ from measured values at the larger angles ranges from 4% in Pb to 10% in Be. We feel that a generous estimate of the uncertainty is ±4% in σ_a.

For high-Z elements, a small correction has been applied to take account of the electrostatic attraction of the pion by the nucleus. At this energy where $\lambda\!\!\!^{-}$ is small compared to nuclear dimensions, the deflection of the orbits can be treated classically. The correction factor[9] is $[1-2Ze^2/RE]$ which, for example, reduces σ_a in Pb by 2.8%.

For $\bar{\sigma}=33$ mb, the weighted average of the free pion-nucleon cross sections, we have computed the expected absorption cross sections for a Fermi distribution with various values of the parameter c. Figure 7

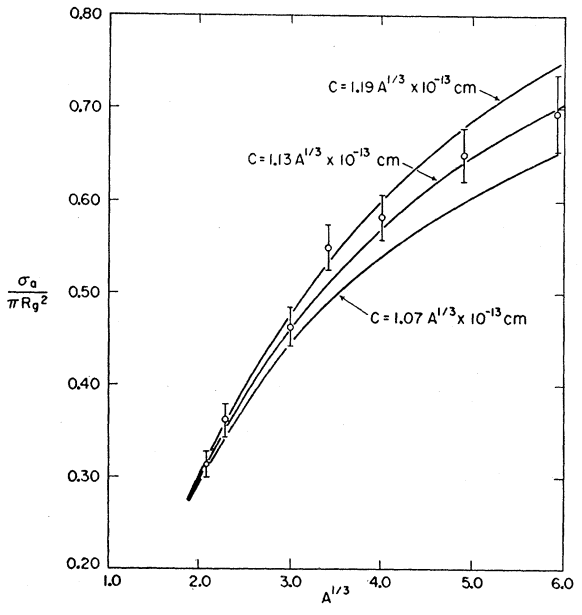

FIG. 7. A comparison of the experimental absorption cross sections with the Fermi tapered model. The cross sections are divided by πR_g^2 where $R_g=(1.13A^{\frac{1}{3}}+2.116)\times10^{-13}$ cm.

[15] K. Gatha and R. J. Riddell, Jr., Phys. Rev. 86, 1035 (1952).

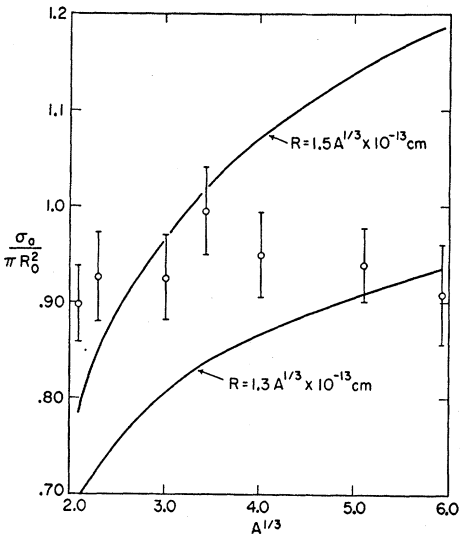

FIG. 8. Comparison of experimental σ_a with a uniform model. All cross sections are divided by πR_0^2 where $R_0=1.3A^{\frac{1}{3}}\times10^{-13}$. Computed curves of the uniform model are displayed for radii of $R=1.3A^{\frac{1}{3}}\times10^{-13}$ cm and $R=1.5A^{\frac{1}{3}}\times10^{-13}$ cm.

shows a comparison of the measured and computed values. The experimental cross sections are a good fit to the shape of the computed curves. The best value of the radius parameter is $c=(1.14\pm0.04)A^{\frac{1}{3}}\times10^{-13}$ cm.

The heavy elements are the most strongly weighted in the determination of c. They are insensitive to the value of $\bar{\sigma}$ since $d\sigma_a/\sigma_a=0.2d\bar{\sigma}/\bar{\sigma}$ for Pb. On the other hand, the light-element cross sections are insensitive to c but are quite sensitive to $\bar{\sigma}$. For example, $d\sigma_a/\sigma_a=0.6d\bar{\sigma}/\bar{\sigma}$ for carbon. Thus for the model, in addition to the radial parameter c obtained from the heavy elements, the light elements give an experimental measure of $\bar{\sigma}$ which is quite insensitive to the value of c. If c lies in the range 1.07 to $1.19A^{\frac{1}{3}}\times10^{-13}$ cm, the C and Be experimental values yield the result $\bar{\sigma}=34\pm3$ mb, which is clearly in excellent agreement with $\bar{\sigma}=33$ mb obtained from the free pion-nucleon cross sections.

In Fig. 8, the measured values of σ_a are compared to those computed for a uniform distribution with $R=1.30$ and $1.50A^{\frac{1}{3}}\times10^{-13}$ cm. It is clearly not possible to fit the shape of the experimental points with a single parameter of the form $R=r_0A^{\frac{1}{3}}$. A reasonable fit to the data can be obtained for a uniform distribution in the form $R=[r_0A^{\frac{1}{3}}+b]$ with $r_0=b=1.11\times10^{-13}$ cm although there is no evident reason to choose a distribution of this form.

The radial parameter $c=1.14A^{\frac{1}{3}}\times10^{-13}$ cm which gives the best fit to the Fermi distribution is 6% larger than that obtained from electron scattering.[8] Such a difference could well be the result of the finite range of the pion-nucleon interaction. The range of interaction can be considered in a phenomenological manner[14] by describing the probability of an interaction between a nucleon at position $\mathbf{r}$ and a pion at position $\mathbf{r}'$ by a function $F(\mathbf{r}'-\mathbf{r})$. Then if F is normalized to unity, an effective nuclear density $\rho'(r')$ may be obtained by "folding in" $F(\mathbf{r}'-\mathbf{r})$ with the nuclear density obtained from electron scattering: $\rho'(r')=\int\rho(r)F(\mathbf{r}'-\mathbf{r})d^3\mathbf{r}$. The effective density has been computed for a square well interaction; $F(\mathbf{r}'-\mathbf{r})=[(4\pi/3)a_0^3]^{-1}$ for $|\mathbf{r}'-\mathbf{r}|<a_0$, $F(\mathbf{r}'-\mathbf{r})=0$ for $r>a_0$, and a_0 is the range of interaction. The absorption cross section has been computed for $c=1.08A^{\frac{1}{3}}\times10^{-13}$ cm and various values of a_0. For $a_0=1.0\times10^{-13}$ cm one obtains the measured Pb cross section. This is in agreement with the radius of interaction for elementary pion-nucleon collisions obtained by Walker *et al.*[16]

B. Diffraction Cross Section

Table III gives the measured values of σ_d at 970 Mev for the light elements; Table IV gives σ_d in carbon at various energies. To obtain σ_d, the function $f_d(\theta)$ used was that appropriate for the Fermi distribution which fits best the values of the absorption cross section.

The error is estimated by noting that σ_d is essentially obtained by subtracting the deduced value of σ_a from the measured cross section at small angles; $\sigma_d\cong(\sigma_m-\sigma_a)/f_d(\theta)$. The error in σ_a, discussed in detail before, is the principal source of error in σ_d, thus $\Delta\sigma_d\cong\Delta\sigma_a/f_d(\theta)$. The variation in $f_d(\theta)$ by changing the parameter c within the range allowed by the fit to σ_a leads to an uncertainty of $\pm3\%$ and is therefore negligible in comparison.

Values of σ_d and σ_d/σ_a have also been calculated for the various elements. They depend on the real, as well as the imaginary potential through the parameters k_1/K and $\bar{\sigma}$ defined in Sec. III. Curves of σ_d/σ_a are plotted in Fig. 9 with k_1/K as a parameter. The real parts of the pion-nucleon forward scattering amplitude deduced from dispersion relations lead to k_1/K about 0.05. The experimental points all lie somewhat above the predicted curve. Although the errors on each point are large, taken together they lead to a best value of $k_1/K=0.40\pm0.15$. Thus the experimental diffraction cross sections appear to indicate a larger real potential than that predicted from the free pion-nucleon cross sections and the dispersion relations. If σ_d is deduced by assuming a uniform distribution of nucleons, this conclusion is not altered.

The reason for this discrepancy is not clear. Although we feel that the errors assigned are generous, it is to be

TABLE V. Comparison of experimental pion and proton absorption cross sections with the predictions of the optical model.

Element	$\bar{\sigma}(\pi)$ in mb	$\bar{\sigma}(p)$ in mb	$\delta=[\sigma_a(p)-\sigma_a(\pi)]/\sigma_a(\pi)$ Predicted	Experimental
Al	35.7	39.7	+0.06	−0.006±0.038
Ca	35.5	40.0	+0.06	+0.024±0.043
Pb	36.6	38.4	+0.01	+0.017±0.046

[16] Walker, Hushfar, and Shephard, Phys. Rev. **104**, 526 (1956).

noted that almost all systematic errors are in a direction to make the measured σ_d appear larger than the true value. For example, in the discussion of multiple Coulomb scattering, given before, an upper limit to the beam lost by this process was placed at 0.5%. If the loss were this large, it would increase the apparent value of σ_d by 10% in Be and 20% in Ca. Nevertheless, the results do suggest that there may be an effective real pion-nucleus potential several times larger than that predicted by dispersion theory. More precise experiments will be required to verify this conclusion.

C. Dependence of σ_a on Energy

Table IV gives the measured values of σ_a for carbon as a function of kinetic energy. They are deduced in the same way as those given in Table III.

According to the optical model, the energy dependence of σ_a depends only upon the energy dependence of $\bar{\sigma}$. Carbon was chosen for the measurement since it is sensitive to changes in $\bar{\sigma}$; $d\sigma_a/\sigma_a=0.6d\bar{\sigma}/\bar{\sigma}$. Table IV gives the values of $\bar{\sigma}$ at corresponding energies and the absorption cross sections calculated from them.

The measured absorption cross sections are in very good agreement with the calculated values. At 600 Mev, σ_a is somewhat smaller than at higher energies which reflects the lower value of $\bar{\sigma}$ at this energy.

D. Comparison of Pion and Proton Absorption Cross Sections

In Table II, values of the absorption cross section measured at each of two "poor geometry" angles are given for negative pions and protons of 1500-Mev/c momentum in Al, Ca, and Pb. For comparison purposes, it was convenient to choose the same momentum since the angular dependence of the diffraction scattering and the multiple Coulomb scattering are the same. Moreover, the comparison requires no change in the apparatus other than a reversal of the direction of current in the magnets. Thus the relative absorptions are more precise than the absolute values. The results of the measurements at the two angles allow us to state that, within the error, the angular dependence of the inelastic secondaries is the same for pions and protons.

For the purpose of comparing with predictions ofthe optical model, the values of $\delta=[\sigma_a(p)-\sigma_a(\pi^-)]/\sigma_a(\pi^-)$ are given in Table V. The experimental values have been corrected for the electrostatic effect explained in Sec. VA. A 3% error has been included due to uncertainty in the muon contamination. The same optical-model parameters used to fit the absorption cross sections at 970 Mev have been used to obtain the predicted values of δ. The values of $\bar{\sigma}$ for protons were obtained from Chen *et al.*[17]

The experimental values of δ for Al and Ca are somewhat smaller than the predicted values but are scarcely outside the error. A small error should also be attached to the predicted δ from uncertainties in the free cross sections. We conclude that the experimental results are reasonably consistent with the optical model using the free pion-nucleon and proton-nucleon cross sections to obtain $\bar{\sigma}$. Some small corrections to $\bar{\sigma}$ which are in a direction to improve the agreement are discussed in the next section.

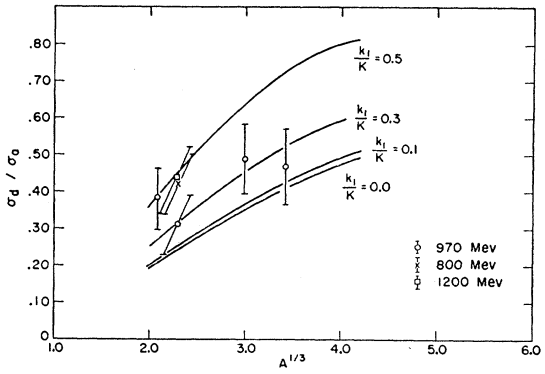

FIG. 9. A comparison of the measured values of σ_d/σ_a to those calculated from the Fermi distribution for various values of the parameter k_1/K. The dispersion theory gives $k_1/K=0.05$.

The very recently reported work of Booth *et al.*[1] for incident protons of 900 Mev can be directly compared to our results at nearly the same energy. For Al and Pb, the measured absorption cross sections at each angle are within the experimental errors quoted. The tendency for light elements like Al and Ca to give a smaller cross section than that predicted from the Fermi distribution as noted above is even more pronounced for their values in C. These lower cross sections in the light elements allow them to fit a square-well potential with $r_0=(1.26\pm0.03)\times10^{-13}$ cm, which does not seem to be possible for pions (see Fig. 8). A correction for the Pauli exclusion principle tends to reduce this difference.

E. Corrections to $\bar{\sigma}$

As is well known, there are two corrections which should be applied to the value of $\bar{\sigma}$, which in the above discussion was obtained directly from the elementary pion-nucleon cross sections. They are (1) a correction for the effect of the Pauli exclusion principle which reduces $\bar{\sigma}$, and (2) a correction for the direct absorption of pions which tend to increase $\bar{\sigma}$.

The Pauli exclusion principle forbids collisions in which the energy transferred to the struck nucleon in an elastic collision is too small to raise it to an unoccupied state. To estimate this effect, we treat the nucleus as a Fermi gas and suppose that collisions are inhibited for which the momentum transfer is less than the maximum Fermi momentum k_F. This effect prevents scattering in a solid angle $\pi(k_F/k_0)^2$ about the forward direction. The correction to $\bar{\sigma}$ is $\Delta\bar{\sigma}=-\pi(k_F/k_0)^2[d\sigma(0)/d\Omega]$. The

[17] Chen, Leavitt, and Shapiro, Phys. Rev. **103**, 211 (1956).

forward differential elastic cross sections are known[5,18] and we take $k_F=200$ Mev/c. The resulting correction reduces $\bar{\sigma}$ by about 10%.

The value of $\bar{\sigma}$ derived from elementary pion-nucleon processes does not include the possibility of direct absorption by two or more nucleons. Reactions such as $\pi^-+p+n\rightarrow n+n$ and $\pi^-+p+p\rightarrow p+$n are known to be very important at low energies. These reactions are discussed by Brueckner, Serber, and Watson.[19] They have shown that the direct absorption cross section in heavy nuclei is given by a factor Γ times the cross section for the reaction $\pi^-+d\rightarrow n+n$. The factor Γ which depends only on the structure of the nucleus is essentially the ratio of the probability for finding two nucleons close together in a nucleus to that in the loosely bound deuteron. An analysis of the low-energy experimental data gave $\Gamma\approx 10$.

We can obtain an estimate of the direct absorption cross section in deuterium by detailed balancing. If we assume charge symmetry, the cross section of $\pi^-+d\rightarrow n+n$ for 1370-Mev pions is equal to that for $p+p\rightarrow\pi^++d$ with 3-Bev protons. The present data, though very crude, indicate this cross section is roughly 0.5 mb.[20] Thus the π^--p cross section in nuclear matter should be increased by ≈ 5 mb, which would increase $\bar{\sigma}$ by 2.5 mb to take account of direct absorption processes.

The above considerations show that the two corrections are approximately equal in magnitude but opposite in sign. Therefore, for pions our use of $\bar{\sigma}$ derived from the free cross sections is justified. However, since there is no direct absorption of protons analogous to that for pions, $\bar{\sigma}(p)$ should be reduced relative to $\bar{\sigma}(\pi)$ by about 10% to compare proton and pion absorption cross sections as in Sec. VD. Indeed, this correction is in the direction necessary to improve the agreement between the measured and computed pion and proton absorption cross sections. The data are consistent with a correction of this magnitude.

[18] Morris, Fowler, and Garrison, Phys. Rev. **103**, 1472 (1956).
[19] Brueckner, Serber, and Watson, Phys. Rev. **84**, 258 (1951).
[20] Block, Harth, Cocconi, Hart, Fowler, Shutt, Thorndike, and Whittemore, Phys. Rev. **103**, 1484 (1956).

VI. SUMMARY

Measurements of the absorption cross section in nuclei for high-energy pions have been compared to the predictions of the optical model. The measurements which were made were chosen in order to vary asmany of the parameters entering into the model as was experimentally feasible. They included the following: (1) for elements from Be to Pb, σ_a at 970 Mev; (2) for C, σ_a between 600 and 1200 Mev; and (3) for Al, Ca, and Pb, σ_a for 1500-Mev/c negative pions and protons.

All of the measurements of σ_a are completely consistent with a potential having the shape of the Fermi distribution and a single radial parameter $c=(1.14\pm 0.04)A^{\frac{1}{3}}\times 10^{-13}$ cm. The shape of this potential is consistent with that required for the nuclear charge distribution as determined from electron-scattering data. The parameter c is, however, 6% larger than the best value for that of the charge distribution. This difference is well accounted for by a range of the pion-nucleon interaction equal to $\approx 1\times 10^{-13}$ cm, which is also the value deduced from the elementary pion-nucleon interaction. The experimental absorption cross sections will not fit a uniform potential with one parameter $R=r_0A^{\frac{1}{3}}$.

The measured diffraction cross sections are 20–30% larger than those predicted by the optical model. This result indicates that for pions the real potential of the nucleus may be several times larger than the value deduced from the optical model and the dispersion theory. It is conceivable that the discrepancy may be due to an unknown systematic error in the measurement. Further experiments will be necessary to verify the existence of such a potential.

ACKNOWLEDGMENTS

It is a pleasure to acknowledge helpful discussions with Professor R. Serber, Professor K. A. Brueckner, Professor R. J. Glauber, Professor R. W. Williams, and Dr. O. Piccioni.

We wish to thank Dr. S. A. Goudsmit and Dr. G. B. Collins for their encouragement and support, and the operating staff of the Cosmotron for their cooperation.